Cardiac Cycle Phase Detection using an Artificial Neural Network

Sangameswaran. N[1] Dr. P. Meenakshi Devi[2]
[1,2]Department of Computer Science & Engineering
[1,2]KSR Institute for Engineering and Technology

Abstract— this paper proposes a new hybrid approach to estimate the cardiac cycle phases in 2-D echo-cardiographic images as a first step in cardiac volume estimation. The cardiac cycle phase identification has done by making out the anatomical information of the heart with the dataset of both the normal and infant cardiac images of the heart. These dataset here helps in extracting the information about the given image and also differentiates them under the two categories either the heart left ventricle is in the diastolic state or systole state. For identifying this state the mitral valve position of the heart is considered. In the first step, the noise in the image was removed using the median filter and wavelet transforms for the canny edge detection as the second step. In third step, feature extraction, mean and the standard deviation value for the dataset images were calculated. To classify the two states of the heart, the feed forward back propagation neural network was used in the fourth scenario. By training the neural network, the images of the heart were classified into diastole and systole and could be measured in both the manner and compared.

Key words: Artificial Intelligence, Cardiac Cycle, MATLAB, Image Features

I. INTRODUCTION

The incidence of chronic heart failure in humans is very high and as a result, the morbidity and mortality are alsovery high in all countries, regardless of the economic develop-ment level [1], [2]. The data on mortality caused by the chronic heart failure reveal that the five-year mortality rate remains at an alarmingly high level of 50% [3]. Heart failure is, therefore, a major clinical problem. Echocardiography represents a non- invasive procedure to examine the heart and the surrounding blood vessels [4]. By echocardiography, the physicians visually inspect the four cardiac cavities (left and right atria, left and right ventricle), the inferior vena cava, the aorta, the mitral valve, the aortic valve, the tricuspid valve, and the pulmonary valve. The image of the left ventricle (LV) and the analysis of the cardiac cycle are of great importance to cardiac research and represent a valuable tool to clinically assess cardiac health. The automatic detection of cardiac phases is a first step in the diastolic and sys- tolic volume calculation task. Moreover, the echocardiography also allows for automatic or semiautomatic analysis based on image features. Gaasch and Zile [5] showed that the clinical examination cannot distinguish between diastolic heart failure and systolic heart failure. Instead, the instrumentality of the echocardiography makes it possible. Ramachandran et al. [6] used the optical flow technique to reveal the displacement between few control points set on the left ventricular wall in short-axis view along the cardiac cycle. They established a relationship between the magnitude of displacement and the ECG recording. Negrini et al. [7] kinetically analyzed the wall in each frame of the cardiac cycle in order to gather information about contractility and diastolic functions. They used the automatic detection of the LV contours through the cardiac cycle phases. Their method involves a threshold operation and a spatial filtering followed by an automatic ventricular contour tracking. Aase et al. [8] investigated the automatic detection of the QRS complex and also the automatic cardiac cycle separation in B-mode echocardiographic images. Their method is based on a curvature in terpretation of the mitral annulus displacement identified by a deformable B-spline curve. The generic echocardiographic timing algorithm (GETA) was used to analyze the mitral annulus curve displacement and to estimate the time point of cardiac cycle start. Kachenoura et al. [9] proposed a combination of two methods to automatically detect the end diastole and end systole. The first method is based on the mean intensity variation in a region of interest (ROI) during the cardiac cycle. The second method uses the correlation coefficient values between the end diastolic image and the next frames in the cardiac cycle. Martin et al. [10] presented a semiautomatic method for the segmentation and the tracking of the mitral valve leaflet in both phases of cardiac cycle. The main drawbacks of their method are: 1) the inability of the algorithm to accomplish the segmentation when motion of the muscle is very fast, going from an image to the following one and 2) the necessity of manual initialization of active contour model (called "the snake") on the first image of the sequence.

All the traditional segmentation algorithms alone require significant user interaction to segment LV and they have been combined with other segmentation techniques in hybrid schemes to minimize user intervention. These algorithms work for midventricular view of LV, but have problems in basal and apical view. Based on this general finding, this paper proposes a new algorithm able to accurately estimate the cardiac cycle phases in echocardiographic images without involving any manual tracing of the boundaries for segmentation process. To the authors' best knowledge, the hybrid method proposed in our study is the first approach of such a technique. Our attention was mainly focused on the left ventricular cardiac chamber. The purpose of the study was to increase the recognition ability of the algorithm, so that it correctly discerns between atrial systole and atrial diastole. Detailed cavity geometry and the position of the mitral valve were assessed using denoising, binarization, and edge detection techniques. The denoising operation was performed in the framework of additive Gaussian and multiplicative noise described by Rayleigh distributions. Our goal is not to develop a new denoising algorithm but to optimize the formalism for denoising images and to preserve anatomical details relevant from the clinical point of view. To characterize the cardiac cycle phases, an original set of features was proposed and derived. The mitral valve position was described in terms of three image features: 1) the number of boundary pixels belonging to an identified boundary; 2) the height of the mobile rectangle mask which enclosed the useful contour pixels; and 3) the horizontal size of object's boundary inside

the mask. Image features were defined and computed for each image in our dataset by using edge detection. Finally, an artificial neural network (ANN) has been trained as a classifier for effective detection of the mitral valve position in the echocardiographic images. Our method does not require the user intervention. Moreover, this hybrid method allows improving the time efficiency. The main reason underlying this study arises from the finding that if the mitral valve annulus fails to properly connect with the leaflets, then the functioning of the heart may be compromised resulting in the mitral valve regurgitation and stenosis heart affection.

This paper is organized as follows. Section II describes the methods and techniques employed here and it also introduces a new recognition algorithm. Section III provides the experimental results and discussions. Finally, the conclusions and ideas for further developments are outlined in Section IV.

II. METHODS

A. Experimental Algorithm and Case Sample:

Fig. 1 presents the flowchart of the proposed algorithm. The algorithm contains three parts. In the first part, the images are processed using the denoising, binarization, and segmentation techniques. A set of image features was extracted in the second part. In the third part, each component of the feature vector was assessed for both the analyzed cardiac phases, and then the images belonging to our database were classified by the instrumentality of an ANN. The cardiac cycle phase estimation is performed in apical two-chamber long-axis 0◦ view (LAX0) of 2-D echocardiographic images.

In order to evaluate the capability of our method to noninvasively gather all information about the position in motion of the mitral value, frames of cine ultrasound data of human heart were used.

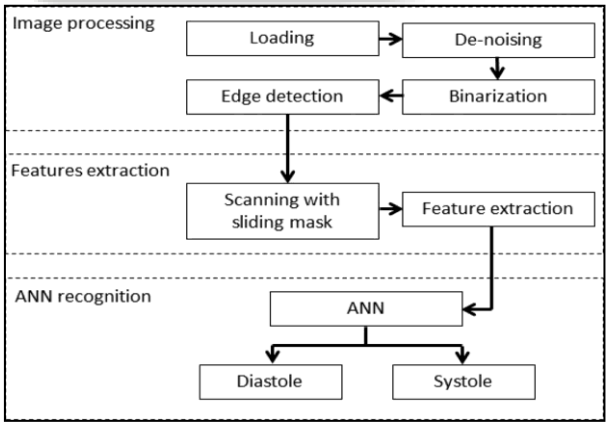

Fig. 1: Flowchart of the Algorithm

One hundred and fifty images that include both nor- mal heart and infarct cardiac pathology were used. The infarct pathology has been chosen because it could be the cause of mitral valve regurgitation when the valve orifice is too wide to close properly. Also, dead tissue and scarred tissue which may occur after myocardial infarction do not contract and impaired on the mitral valve position.

All images were acquired in vivo using the VIVID E9, GE HORTEN MOK WAY scanning systems (functioning in the Laboratory of Cardiovascular Imaging and Dynamics, Catholic University of Leuven, Leuven, Belgium). The 256 × 256 pixels images with 8 b/pixel DICOM were used. The hardware of the experimental environment was an Intel (R) Core (TM) 2 Duo CPU T 5900, 2.20 with 3-Gb RAM, operating Toolbox Processing Image and Neural Networks within MATLAB R2009a (the Mathworks Inc., Natick, MA). The statistical data analysis was performed using the SPSS ver.17 software (SPSS Inc., Chicago, IL).

B. Image Denoising:

Removal of noise is shown to be a crucial step in imaging cardiac disease diagnosis. An efficient method for accurate noise filtration of the echocardiographic images is based on the Fourier transform (FT) and Gaussian low-pass filter (GLPF) [11], [12]. Here, the image processing is a three-step process: 1) the FT (1) is performed; 2) filtering the frequency components by using the GLPF (2); and 3) the inverse FT (3) is computed in order to reconvert the image to the spatial domain. Smoothing is achieved in the frequency domain by dropping out the high-frequency components and it is commonly used in edge detection when the algorithms are sensitive to noise

Here, f (x,y) denotes the processed image, M and N denote the image resolution, F (u,v) is the FT result, H (u,v) is the filter transfer function corresponding to the GLPF, F (u,v) stands for the result of convolution between F and H functions, g(x,y) is the inverse FT (that is the denoised image), D(u,v) represents the distance from the point (u,v) to center of filter, and D0 represents the parameter that is a nonnegative number associated with the standard deviation. The quality of the denoising process with FT and GLPF is strongly dependent on the value of the D0 parameter. To assess the performance of the denoising process, we performed our test in two scenarios (where we assumed that both the additive Gaussian and the multiplicative Rayleigh noise exist in the images) by using a subset randomly chosen from our dataset. The goal is to compare the optimal way to denoise images. Also, we avoided using the synthetic images in order to establish the optimum value of the D0 parameter. Because we cannot find "noise-only" images, we generated noisy images by adding the noise into images, and we calculated the optimal D0 value that minimizes the restoration error. D0 is used on the input images during the noise removal operation. Various values of mean and variance parameters were used during this operation.

The noise quality parameters, such as the signal-to-noise ratio (SNR), the peak signal-to-noise ratio (PSNR), the mean squared error (MSE), and mean absolute error (MAE) [11], [13], rep- resent the quality indicators of the denoising process. A better denoising is characterized by higher values of SNR and PSNR parameters and lower values of the MAE and MSE parameters.

C. Binarization Methods:

Otsu's global binarization method was employed in order to automatically obtain a single optimal binarization thresh-old [14]. This technique divides the histogram of the image into two classes and calculates the optimum threshold T that separates these two classes so that their combined spread (intraclass variance) to be minimal.

D. Image Segmentation and Edge Detection:

Canny detector is looking for intensity discontinuities but it provides too many possible boundaries. It produces spatially extended outputs and we used these outputs to reduce the search space by selecting a satisfactory contour. A threshold value N is chosen in order to hold the core bound- ary (when the contour pixel number is higher than N) and to discard those boundaries classified as isolated (for which the contour pixel number is lower than N).

E. Feature Extraction:

In our study, the classification process is not globally focused on the entire image of the LV. To classify the position of the mitral valve, an ROI with rectangular shape has been identified. The entire image is scanned by using a mobile rectangular mask with height of H pixels and width identical to the image width. The coordinates of the left corner of the sliding mask are (1, h), where h ∈ [1, image height − H + 1]. The scanning process identifies the regions of interest. ROIs consist of those rectangle areas which contain the highest number of contour pixels. The proposed image feature vector has two elements p = [p1 p2]T . p1 is the maximum number of contour pixels (within the rect- angle mask) used for computation and p2 represents the biggest horizontal length of the individual contours which are present inside the rectangular interest area. p2 is used to eliminate the small false regions.

F. Statistical t-Test:

To validate the discernibility between the p1 and p2 feature classes of dataset belonging to two cardiac cycles, the t-test analysis was used [17]. The p value is a useful parameter able to discern whether the means of the two samples are significantly different.

G. Artificial Neural Network:

We consider an ANN as a classifier. The artificial neuron is inspired from real biological neuron model, which is formed by dendrites (inputs), body, and axon (output). A multiple input neuron consists of inputs p=[p1 p2 …pR]T, (vector) the weight vector w= [w1,1 w1,2 … w1,R] the bias b, the summation, which performs a linear combination of in-puts, and the transfer function f which produces the scalar output a (see Fig. 2) [16].

The neuron output is calculated as

$$a = f(wp + b) \qquad (4)$$

In this study, the symmetric hard limit transfer function (or "hardlims") from the Neural Network Toolbox of the MATLAB software was employed. This function forces a neuron to output +1 if its net input reaches a threshold. Otherwise, it outputs –1. In order to solve the problem of two classes (diastolic and systolic phases) of the input vector, we need a perceptron with two neurons.

The supervised learning procedure involves that the ANN must learn using a training dataset, consisting of particular in- put vectors and predicts output values. Compared with statistical methods, the ANN needs less training data for an accurate analysis.

III. Results and Discussion

The experimental images were divided into two sets corresponding to two analyzed cardiac cycles (systole and diastole) by one expert radiologist physician. The expert manually labeled the images. This activity is labor-intensive and tiring. Note that the expert's accuracy was 100%. Seventy-five systolic images and seventy-five diastolic images were used. The experimental echocardiographic images came from a blend of healthy and cardiac patients that suffer from myocardial infarction.

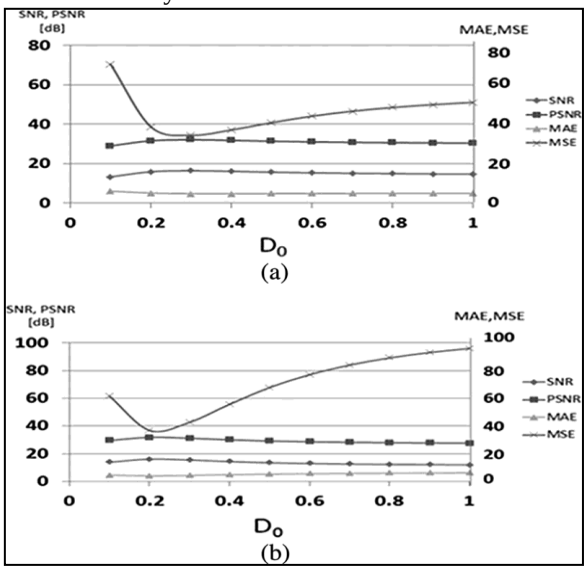

Fig. 3: Diagrams of the noise quality parameters when (a) Gaussian noise or (b) Rayleigh noise with mean 0.1 and variance 0.002 were added. The denoising operation uses FT and GLPF

The optimal parameter of this approach can be either a maximum or a minimum, depending on the quality parameters of the noisy images. Fig. 3(a) and (b) presents the evolution of SNR and PSNR values (measured in dB) and of MAE and MSE values, respectively, during the denoising process.

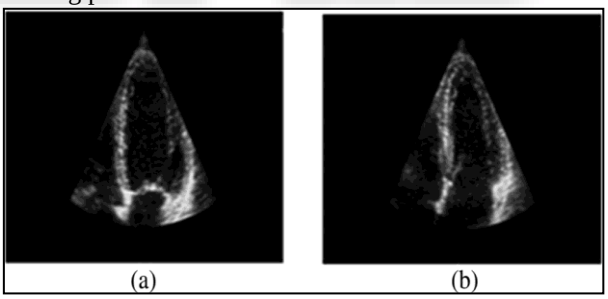

Fig. 4: Denoising results using FT and the GLPF with D0 = 0.3. (a) Atrial diastole. (b) Atrial systole.

Fig. 5: Images binarized using the Otsu method. (a) Atrial diastole. (b) Atrial systole.

For additive Gaussian noise, an average optimal D0 = 0.3 was obtained by computing the optimal values characteristic to qualitative diagrams for each particular denoised experience.

All experimental images were denoised using the FT and GLPF. Fig. 4 shows the denoised images using FT and GLPF at D0 = 0.3. Fig. 5 presents the binarized images using the automatic Otsu method. The binarization produces satisfying results and the myocardium walls are optimally highlighted.

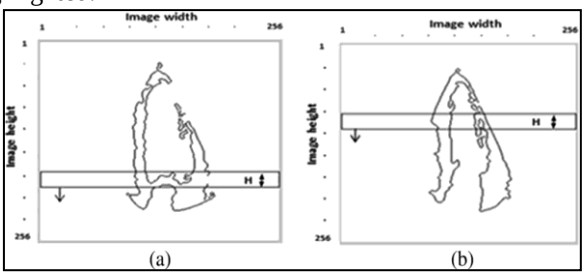

Fig. 6: Edge Information by Canny Detector and the Rectangular Scanning Window. (A) Diastole. (B) Systole.

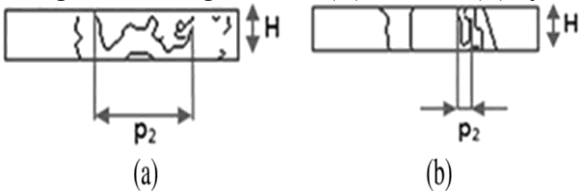

Fig. 7: Example of the selected ROI identified in Fig. 6(a) and (b).

Diastolic phase		Systolic phase	
p_1	p_2	p_1	p_2
215	23	135	17
157	46	163	20
195	44	180	19
172	31	178	16
203	48	156	10

Table 1: Examples of the Values Corresponding To the Proposed Features

The image segmentation covers the contour-based approaches, and tries to exploit curvilinear continuity characteristics of the analyzed mitral valve structures.

Fig. 6 shows the edges detected by using the Canny method. Most of the major edges were detected but also lots of details have been emphasized and this can hamper the subsequent processing. In order to identify the position of the mitral valve, these images were scanned with a horizontal rectangle window having height H. Fig. 7 shows examples of regions of interest that include the maximum number of the contour pixels used to describe the position of the mitral valve.

ROIs considered in our analysis contain the maximum number of contour pixels (p1 value). For diastolic phases, this condition is always accomplished when the mask scans the mitral valve in closed position. The mask will detect those regions containing the higher number of contour pixels, as Figs. 6(b) and 7(b) present. This drawback is minimized by using the second feature, p2 , which helps the ANN to classify the images as diastole for higher value of p2 and as systole for lower value of p2 . Table I presents certain examples of the proposed features.

Statistical feature	p_1 of diastolic phase versus p_1 of systolic phase	p_2 of diastolic phase versus p_2 of systolic phase
Mean ±standard deviation	186±22 vs. 171±21	30±13 vs. 16±8
p-value	0.032	<0.001

Table 2: Results of the Statistical T-Tests

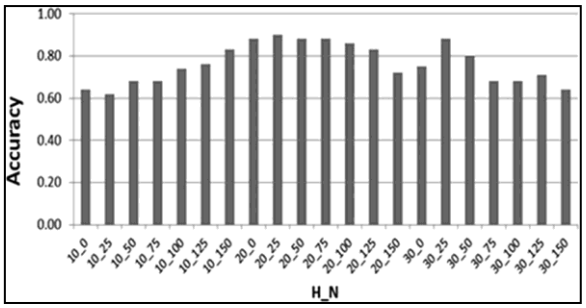

Fig. 8: CADi accuracy versus various combinations of H and N parameters.

The higher accuracy corresponds to the (20; 25) combination. p1 of diastolic phase versus p1 of systolic phase and 2) p2 of diastolic phase versus p2 of systolic phase. The t-test results referred to the mean ± standard deviation and the p-value are presented in Table II. They confirm the significant differences between p1 and p2. The recognition and classification results are strongly influenced by N (the threshold of Canny edge detector) and H (the height of sliding window) parameters. To obtain the threshold N value, the following idea is developed. As Figs. 6(b) and 7(b) show, when the mask scans LV in the systolic phase, the presence of the small, independent contours or edges having the contour pixel number lower than the threshold N leads to an increase of the feature p1 value. Therefore, the recognition process failed and the image will be misclassified as diastole. On the other hand, when higher values of the threshold N were used, then the small, independent contours were removed. As a result, the value of the p1 feature decreased and the diastolic images were misidentified as systolic images. Concerning the height H of the scanning mask, the analysis presented in the following was made. If H has low values, the mask could fail to include the entire contours orientated more or less horizontal and finally, the values of the p2 parameter are low in diastolic phase images and a misclassification as systole can result. The higher H value of the rectangle mask would lead to overestimate the values of both p1 and p2 parameters and the final result is the misclassification of both systole and diastole analyzed cases.

In order to establish the optimal values of the H and N parameters, the accuracy of the CADi application for various combinations of H and N parameters was computed (see Fig. 8). Based on this analysis, the optimal values of H = 20 and N = 25 were chosen. To provide reliable results during the classification process, the ANN needs to be trained.

No.	Diastole dataset			Systole dataset		
	p_1	p_2	Classification result	p_1	p_2	Classification result
1	0.83	0.57	diastole	0.59	0.33	systole
2	0.98	0.48	diastole	0.71	0.44	systole
3	0.62	0.86	diastole	0.68	0.24	systole
4	0.72	0.71	diastole	0.73	0.42	systole
5	1.00	0.57	diastole	0.60	0.35	systole

Table 3: Certain Feature Values Corresponding To the Feature Vectors of Ann

Noise distribution	Sensitivity	Specificity	Accuracy	Precision
Gaussian	90.7 %	89.2 %	90 %	89.3 %
Rayleigh	81.5 %	83.1 %	82.3 %	82.8 %

Table 4: Efficiency of the Cadi System

The training set was composed of ten systolic images and ten diastolic images, randomly chosen from the experimental dataset. The ANN correctly recognized all 20 training images. Table III shows certain examples of the feature vectors corresponding to the experimental images. Both the training and the feature vectors were normalized by their highest values of p1 and p2 , respectively. Our study shows that the ANN enables an accurate distinction between diastole and systole. During the recognition process, 130 test images were investigated and they were equally divided between diastolic and systolic phases. For additive Gaussian noise removed by using the parameter D0 = 0.3, 59 diastolic images were correctly recognized as TP, 6 diastolic images were incorrectly recognized as FN, 58 systolic images were correctly recognized as TN, and 7 systolic images were incorrectly recog- nized as FP. For multiplicative Rayleigh noise and D0 = 0.2, 53 diastolic images were correctly recognized as TP, 12 diastolic images were incorrectly recognized as FN, 54 systolic images were correctly recognized as TN, and 11 systolic images were incorrectly recognized as FP. The recognition failing rate is al- most equally distributed between healthy and infarcted patients so that a possible pathology does not affect the accuracy of results provided by CADi. When taking into account only the diastolic phase, in the first scenario the diagnostic performance of ANN for the differentiation is 90.7% (59/65) accurate. In the case of systole, the differentiation is 89.2% (58/65) accurate. For the second scenario, the sensitivity is 81.5% (53/65) and the specificity is 83.1% (54/65). This finding is readily explained by the entirely different appearance of the mitral valve in closed position. On the other hand, the performance of ANN for differentiating systolic phase is more challenging, because of the more similar appearance of various small detected contour types. At systole, these small independent contours can be easily mistaken as mitral valve, and thus, the false-negative diagnosis of systolic phase is made.

In Table IV, we compare the efficiency of our CADi in both considered scenarios. We obtain, on average, the best results when the algorithm was specifically designed for additive Gaussian estimation. Experimental results show that this scenario is more efficient in removing noise, while preserving edges. Instead, the Rayleigh solution becomes less competitive. Our hypothesis was that what matters is not as much the noise magnitude, but rather the noise distribution.

The experimental results proved good precision and effectiveness of our recognition algorithm in clinical studies. This proposed technique uses expert knowledge to detect the position of the mitral valve and ANN learns from in vivo data and does not need to be reprogrammed. Once ANN is trained, the detection becomes very fast. The calculated work time necessary to totally investigate an experimental image is 2±0.3 s so that the proposed CADi application facilitates a real-time classification. In routine practice, determination of systole and diastole frames is visual through slow animation of loops with a trackball. The manual labeling activity takes between 4 and 6 s per image.

Our approach is a new proposal for a well-known task, and thus, the proposed method cannot be compared with any other method in terms of accuracy or similarity of the results. We validate our method by systematic comparison of the accuracy in classification application.

We note that the proposed algorithm run only in apical two- chamber long-axis, 0◦ view (LAX0) of 2-D echocardiographic images. Still, it can be extended in the 3-D volumetric images, by capturing additional apical two-chamber long-axis 90◦ (LAX90) views. This approach is a local one and it allows us to save time and resources and to handle it with low amount of processed information. However, we recognize the cha lenges that our study has still to overcome: the standardization and/or the qualification such that it will become a true routine methodology.

On the other hand, taking into consideration all the medical logistic functions and apparatus and user's effort, entirely automatic analysis becomes an attractive idea because it can eliminate the user variability and it can allow for an unsupervised and possible online quantification. In this respect, our proposed methods could be improved and extended. A multiobject out- look incorporating endocardium, epicardium, valves, atria, and vessels will improve the detection accuracy.

IV. Conclusion

A new possible approach in the field of heart disease remote monitoring could offer patients a more individually focused care and, thus, an improved quality of life. The objective of this study was to develop a method capable of real-time estimate the cardiac cycle in LV echocardiographic image sequences. In a first step, the developed system used the denoising, the binarization, and the segmentation techniques. Then, an original method dealing with new proposed image feature sets for an analysis task was designed. In the second step, the ANN technique was employed followed by a CADi efficiency study. In order to obtain a computationally fast and efficient algorithm for cardiac cycle phase recognition, we have proposed a local approach, where an ROI of rectangular shape was identified. The approach presented previously benefits from the advantages of a new hybrid method, which couples additive and multiplicative noise removal with image processing and classification tools. Finally, we have showed that our hybrid strategy and the Gaussian noise distribution constitute a competitive solution for fast estimate of the cardiac cycle phases. An accuracy of 90% sug- gests a good performance of the proposed algorithm when an additive Gaussian noise distribution is considered.

References

[1] W. B. Kannel, "Incidence and epidemiology of heart failure," Heart Fail Rev., vol. 5, pp. 167–173, 2000.
[2] K. Sliwa, A. Damasceno, and B. M. Mayosi, "Epidemiology and etiology of cardiomyopathy in Africa," Circulation, vol. 112, pp. 3577–3583, 2005.
[3] S. Stewart, "Prognosis of patients with heart failure compared with com- mon types of cancer," Heart Fail. Monit., vol. 3, pp. 87–94, 2003.
[4] R. Erbel, "Echocardiography," in Cardiac Imaging: A Multimodality Approach, M. Thelen,

R. Erbel, K. F. Kreitner, and J. Barkhausen, Eds. New York: Thieme Medical Pub., 2009, pp. 34–55.
[5] W. H. Gaasch and R. M. Zile, "Left ventricular diastolic dysfunction and diastolic heart failure," Annu. Rev. Med., vol. 55, pp. 373–394, 2004.
[6] G. Ramachandran, M. Singh, and K. Nityanandan, "Left ventricle wall motion analysis during various phases of cardiac cycle from 2D-echocardiographic images," in Proc. IEEE Eng. Med. Biol. Soc., Oct./Nov. 1991, vol. 13, pp. 235–236.
[7] P. Negrini, P. Tomassini, G. Cella, M. Magrin, M. Ercolani, A. Mazzarisi, V. Gemignani, A. C iampa, P. Marcheschi, and P. Marraccini, "Automatic border detection through a cardiac cycle to analyze left ventricular func- tion," in Proc. Comput. Cardiol. Conf., 2002, pp. 181–183.
[8] S. A. Aase, S. R. Snare, O. C. Mjlstad, H. Dalen, F. Orderud, and H. Torp, "QRS detection and cardiac cycle separation without ECG," in Proc. IEEE Int. Conf. Ultrason. Symp., 2009, pp. 1399–1402.
[9] N. Kachenoura, A. Delouche, A. Herment, F. Frouin, and B. Diebold, "Automatic detection of end systole within a sequence of left ventricular echocardiographic images using autocorrelation and mitral valve motion detection," in Proc. Eng. Med. Biol. Soc. Conf., 2007, pp. 4504–4507.
[10] S. Martin, V. Daanen, J. Troccaz, and O. Chavanon, "Tracking of the mitral valve leaflet in echocardiography images," in Proc. IEEE Int. Symp. Biomed. Imaging, 2006, pp. 181–184.
[11] D. Bibicu, S. Moldovanu, and L Moraru, "Denoising the echocardio- graphic images using Fourier transform," Ann. "Dunarea de Jos" Univ. Galati, Math, Phy, Theoretical Mech., Fascicle II, year III (XXXIV), pp. 73–80, 2011.
[12] R. Gonzales, R. Wood, and S. Eddins, Digital Image Processing Using Matlab. Knoxville, TN: Gatesmark Publishing, 2009.
[13] S. Suryanarayana, B. L. Deekshatulu, K. L. Kishore, and Y. RakeshKumar, "Novel impulse detection technique for image denoising," J. Theor. Appl. Inf. Technol., vol. 5, pp. 102–106, 2009.
[14] W. Hai-Yang, P. De-Lu, and X. De-Shen, "A fast algorithm for two- dimensional Otsu adaptive threshold algorithm," Acta Automat. Sinica, vol. 33, pp. 968–971, 2007.
[15] G. Dougherty, Digital Image Processing for Medical Applications. Cambridge, U.K.: Cambridge Univ. Press, pp. 184–158, 2009.
[16] H. Demuth, M. Beale, and M. Hagan, Neural Network Toolbox 6, User's Guide. The MathWorks, Inc., Natick, MA, 2008.
[17] J. Bailar and D. Hoaglin, Medical User of Statistics. Hoboken, NJ: Wiley, 2009.
[18] S. Moldovanu, L. Moraru, and D. Bibicu, "Computerized decision support in liver steatosis investigation," Int. J. Biol. Biomed. Eng., vol. 6, pp. 69– 76, 2012.

